

Whistler Waves at Venus's Quasi-Parallel Bow Shock

Brent Page¹, Trevor A Bowen², Stuart D. Bale³, John W. Bonnell¹, Anthony William Case⁴, Thierry Dudok de Wit⁵, Keith Goetz⁶, Katherine Amanda Goodrich¹, Jasper S. Halekas⁷, Peter R Harvey⁸, Justin C. Kasper⁹, Davin E. Larson¹, Robert John MacDowall¹⁰, David M. Malaspina¹¹, Mitsuo Oka⁸, Marc Pulupa¹², and Phyllis Whittlesey¹

¹University of California, Berkeley

²Space Sciences Laboratory

³UC Berkeley

⁴Harvard-Smithsonian Center for Astrophysics

⁵CNRS and University of Orléans

⁶University of Minnesota

⁷University of Iowa

⁸Space Sciences Laboratory, University of California, Berkeley

⁹University of Michigan-Ann Arbor

¹⁰NASA Goddard Space Flight Center

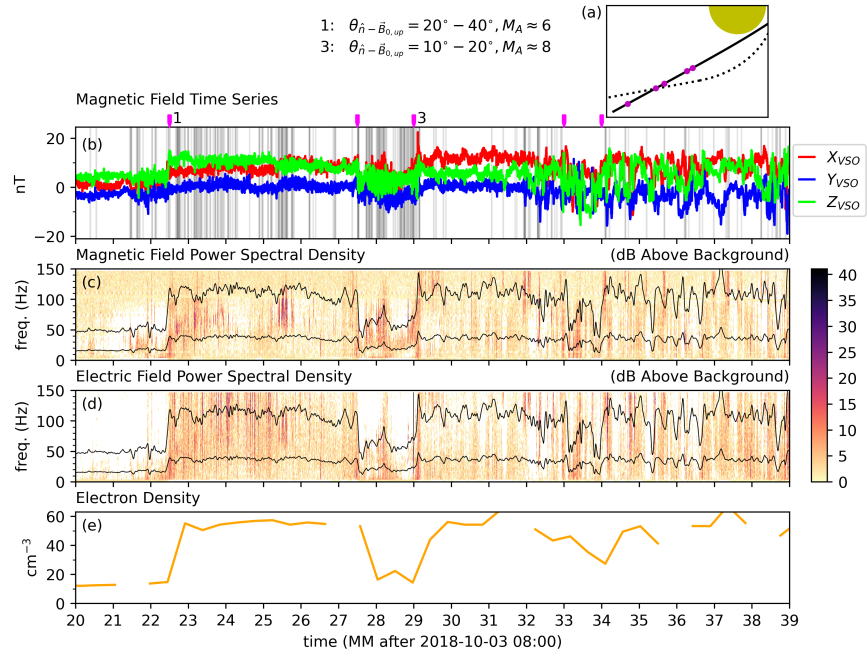
¹¹University of Colorado Boulder

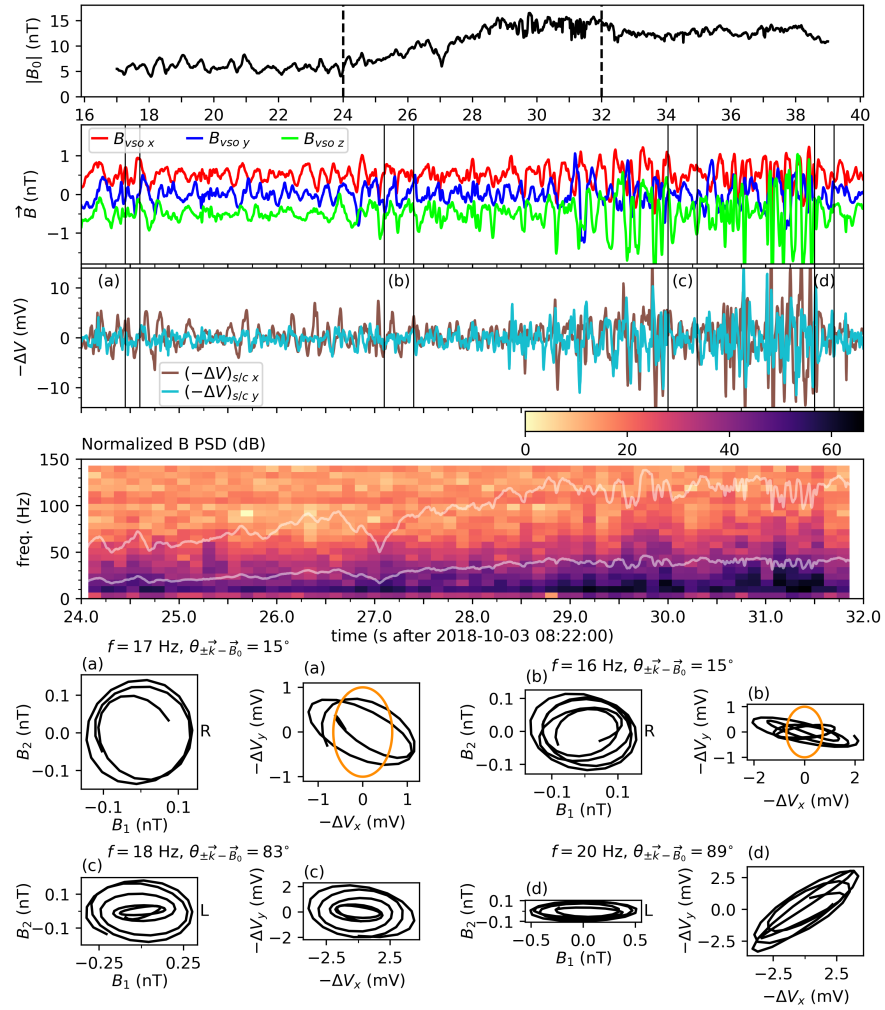
¹²Space Sciences Laboratory, University of California at Berkeley

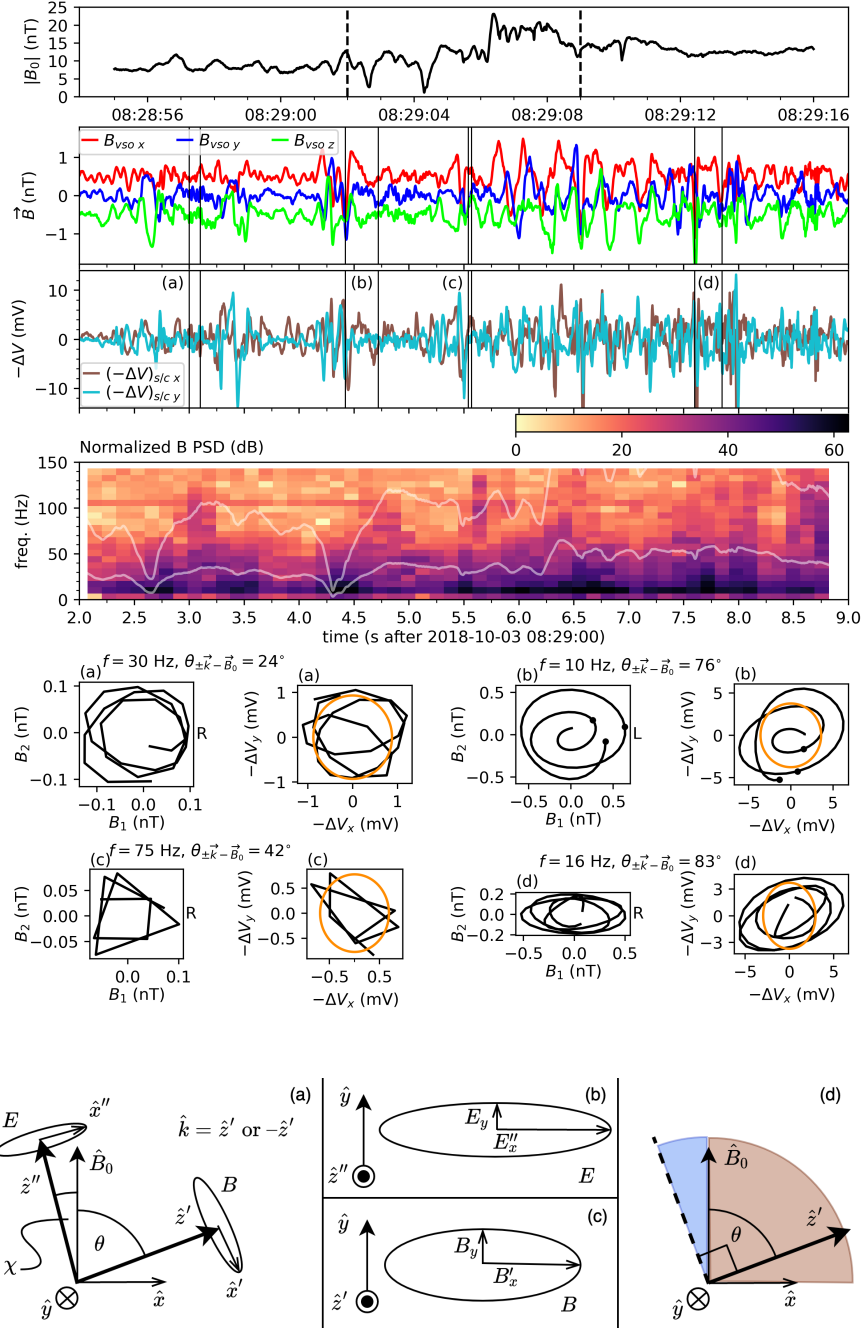
November 23, 2022

Abstract

In planetary bow shocks, binary particle collisions cannot mediate the conversion of upstream bulk flow energy into downstream thermal energy, and wave-particle interactions in part assume this role. Understanding the contribution of waves to shock heating requires knowledge of the modes that propagate in different classes of shocks; we describe the growth patterns of whistler waves within the Venusian bow shock. Waves with frequencies $f \lesssim 0.1 f_{ce}$, where f_{ce} is the electron cyclotron frequency, preferentially grow at local minima in the background magnetic field $|B_0|$. Quasi-parallel propagating whistlers with frequencies between $0.1 f_{ce}$ and $0.3 f_{ce}$ are strongest at the downstream ramps of these $|B_0|$ minima. Immediately downstream of the shock, whistlers with frequencies $f < 0.1 f_{ce}$ propagate more than 80° oblique from \vec{B}_0 and have elliptically polarized \vec{B} fields. A prediction from kinetic theory of the orientation of these waves' \vec{B} ellipses is confirmed to high accuracy.







Whistler Waves at Venus's Quasi-Parallel Bow Shock

B. Page^{1,2}, T.A. Bowen², S.D. Bale^{1,2,3,4}, J.W. Bonnell², A. Case⁵, T. Dudok de Wit⁶, K. Goetz⁷, K. Goodrich², J. Halekas⁸, P.R. Harvey², J.C. Kasper⁹, D. Larson², R.J. MacDowall¹⁰, D.M. Malaspina^{11,12}, M. Oka², M. Pulupa², P. Whittlesey²

¹Physics Department, University of California, Berkeley, CA 94720-7300, USA

²Space Sciences Laboratory, University of California, Berkeley, CA 94720-7450, USA

³The Blackett Laboratory, Imperial College London, London, SW7 2AZ, UK

⁴School of Physics and Astronomy, Queen Mary University of London, London E1 4NS, UK

⁵Smithsonian Astrophysical Observatory, Cambridge, MA 02138 USA

⁶LPC2E, CNRS and University of Orléans, Orleans, France

⁷School of Physics and Astronomy, University of Minnesota, Minneapolis, MN 55455, USA

⁸Department of Physics and Astronomy, University of Iowa, Iowa City, IA 52242, USA

⁹Climate and Space Sciences and Engineering, University of Michigan, Ann Arbor, MI 48109, USA

¹⁰Solar System Exploration Division, NASA/Goddard Space Flight Center, Greenbelt, MD, 20771

¹¹Laboratory for Atmospheric and Space Physics, University of Colorado, Boulder, CO 80303, USA

¹²Astrophysical and Planetary Sciences Department, University of Colorado, Boulder, CO, USA

Key Points:

- Whistler wave growth patterns within the Venusian bow shock have some similarities with those in Earth's bow shock.
- Some whistler waves downstream of the Venusian bow shock propagate at angles more than 80° oblique to the background magnetic field.
- These waves have elliptical magnetic field polarization that is found to be in strong agreement with predictions from kinetic theory.

Corresponding author: Brent Page, brent_page@berkeley.edu

Abstract

In planetary bow shocks, binary particle collisions cannot mediate the conversion of upstream bulk flow energy into downstream thermal energy, and wave-particle interactions in part assume this role. Understanding the contribution of waves to shock heating requires knowledge of the modes that propagate in different classes of shocks; we describe the growth patterns of whistler waves within the Venusian bow shock. Waves with frequencies $f \lesssim 0.1f_{ce}$, where f_{ce} is the electron cyclotron frequency, preferentially grow at local minima in the background magnetic field $|B_0|$. Quasi-parallel propagating whistlers with frequencies between $0.1f_{ce}$ and $0.3f_{ce}$ are strongest at the downstream ramps of these $|B_0|$ minima. Immediately downstream of the shock, whistlers with frequencies $f < 0.1f_{ce}$ propagate more than 80° oblique from \vec{B}_0 and have elliptically polarized \vec{B} fields. A prediction from kinetic theory of the orientation of these waves' \vec{B} ellipses is confirmed to high accuracy.

Plain Language Summary

When particles moving faster than the speed of sound encounter an obstacle, a shock wave forms. This happens, for example, when the electrons and protons streaming away from the Sun flow into planets. When particles pass through a shock wave, their temperature increases and their flow speed decreases. This heating and slowing process is in part mediated by the interaction between collective particle motions (i.e. waves) and individual particles. One type of wave that propagates within and near astrophysical shocks, called a whistler wave, consists of electrons revolving in concert with rotating electric and magnetic fields. This wave is generated in many of the same locations at Venus's shock as at Earth's. Also, the wave's magnetic field rotates in an ellipse instead of a circle when the wave's propagation direction is sufficiently unaligned with the background magnetic field.

1 Introduction

The first examination of whistler waves at Venus was stimulated by measurements from *Pioneer Venus* of 100 Hz electric field power in the planet's magnetosheath (Scarf et al., 1980). These waves were initially suspected to be whistlers, but a lack of coinciding magnetic field measurements prevented definitive mode identification, and they have also been suspected to be lower hybrid waves (Szegö et al., 1991) and ion-acoustic waves (Strangeway & Crawford, 1993).

Venus Express observed 1 Hz circularly polarized magnetic field fluctuations upstream of the bow shock consistent with Doppler shifted whistlers (Orlowski & Russell, 1991; Xiao et al., 2020). These waves have many similarities with 1 Hz waves seen in the corresponding region at Earth, and are thought to grow at the shock and damp out as they propagate upstream.

We focus on whistler waves in the bow shock and compare our observations with those of Pioneer Venus and Venus Express when possible, but primarily use measurements of Earth's bow shock to provide context. Whistler waves have been documented more extensively at Earth than at Venus (e.g. Olson et al., 1969; Holzer et al., 1972; Rodriguez & Gurnett, 1975), and contemporary observatories at Earth such as the Magnetospheric Multiscale (MMS) mission provide a detailed view of wave-fields and particle dynamics (Burch et al., 2016).

Two bands of whistler waves are found in Earth's perpendicular bow shock: one propagating quasi-parallel to \vec{B}_0 with $f > 0.1f_{ce}$ and another propagating oblique to \vec{B}_0 with $f \lesssim 0.1f_{ce}$ (e.g. Y. Zhang et al., 1999; Hull et al., 2012, 2020; Wilson III et al., 2014). The low frequency whistlers are sufficiently strong ($\Delta B/|B_0| \sim 0.1 - 1$) to

73 affect the macroscopic magnetic structure of the shock, and their magnetic field minima
74 are correlated with the higher frequency waves (Hull et al., 2012, 2020).

75 Simulations show that the large $|B|$ gradients of the $f \lesssim 0.1f_{ce}$ waves scatter elec-
76 trons, thereby trapping them in $|B|$ minima, where they have a perpendicular temper-
77 ature anisotropy that may generate the high frequency whistlers (e.g. Oka et al., 2019).
78 The high frequency waves, in turn, scatter electrons via cyclotron resonance (e.g. Oka
79 et al., 2017).

80 *Parker Solar Probe's* (PSP's) measurements in the Venusian shock show a similarly
81 structured spectrum of whistler waves, suggesting that the electron acceleration mech-
82 anisms operating at Earth may also operate here. Similarities in dynamics at Venus and
83 Earth also point to universal processes in magnetized collisionless shocks, insensitive to
84 such factors as the solar wind density, the upstream magnetic field strength, or the pres-
85 ence of a planetary magnetic field.

86 In addition, directly downstream of the shock discontinuity in \vec{B}_0 , PSP's observa-
87 tions reveal whistlers with $f \lesssim 0.1f_{ce}$ that propagate $\sim 80^\circ$ oblique to \vec{B}_0 with mag-
88 netic field ellipticity < 0.6 . The orientations of the semimajor and semiminor axes of
89 these waves' \vec{B} fields strongly agree with predictions from kinetic theory (Verkhoglyadova
90 et al., 2013; Remya et al., 2016).

91 2 Data

92 Although it is primarily designed to study the Sun, PSP will also take measure-
93 ments in the bow shock, magnetosheath, magnetosphere, and upper ionosphere of Venus
94 over seven planned flybys. Each flyby, or Venus Gravity Assist (VGA), transfers some
95 of PSP's orbital energy to the planet, decreasing PSP's distance to the Sun at perihe-
96 lion. We use data from the first VGA, which is illustrated in Figure 1.a.

97 The FIELDS instrument on PSP measures the magnetic field from DC to 293 Hz
98 using two fluxgate magnetometers and from 10 Hz to 50 kHz using a search-coil mag-
99 netometer (Bale et al., 2016). The SCAm data product, which is used for this study, merges
100 the measurements from these two instruments to produce time series data that put high
101 frequency oscillations into the context of the background field variations (Bowen et al.,
102 2020).

103 FIELDS measures the electric field in two coordinate directions using four 2 m an-
104 tennas. They are arranged into two approximately orthogonal dipoles, each consisting
105 of two antennas mounted 3 m from one another. During the time period studied, the Dig-
106 ital Fields Board component of FIELDS continuously sampled these dipoles at 293 Hz
107 (Malaspina et al., 2016).

108 Minimum Variance Analysis (MVA) of the magnetic field is used to determine wave
109 propagation angles relative to the background magnetic field \vec{B}_0 (Sonnerup & Scheible,
110 1998). For an elliptically polarized wave, MVA finds the axis around which \vec{B} is polar-
111 ized, thereby determining \hat{k} with a 180° ambiguity. MVA's results are quoted using the
112 symbol $\theta_{\pm\hat{k}-\vec{B}_0}$, which denotes either the angle between \hat{k} and \vec{B}_0 or the angle between
113 $-\hat{k}$ and \vec{B}_0 - whichever is smaller.

114 The SWEAP instrument suite characterizes the electron and ion populations en-
115 countered by PSP (Kasper et al., 2016). A pair of electrostatic analyzers (SPAN-E) mea-
116 sure the full 3D electron velocity distribution function; we use SPAN-E's estimates of
117 the electron density and temperature (Whittlesey et al., 2020). We also use measurements
118 of the proton density, proton temperature, and bulk plasma velocity from the Faraday
119 cup (SPC) component of SWEAP (Case et al., 2020).

3 Whistler Wave Activity at the Bow Shock

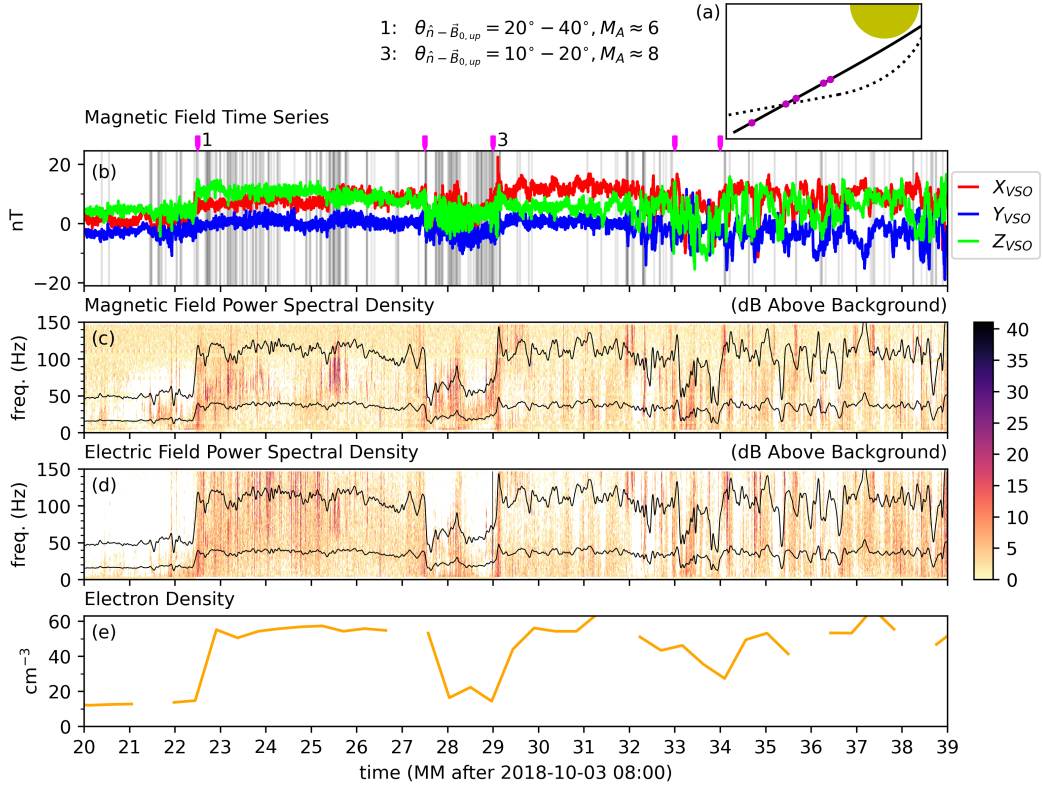


Figure 1. Panel (a): the flyby geometry. The solid black line is PSP’s trajectory; it starts at the bottom left, which is anti-sunward and dawnward of Venus (yellow circle). The trajectory lies approximately in the ecliptic. A global bow shock model from T. Zhang et al. (2008) is shown with a dotted line. The bow shock locations from PSP’s flyby are marked by purple dots, which correspond to the purple hashes above panel (b). We focus on the bow shock crossings labeled 1 and 3, whose shock normal angles and Alfvén Mach numbers are listed at the top of the Figure. The magnetic field in panel (b) is in VSO coordinates, and the gray shading marks locations of whistler waves. Panel (c): The power spectral density (PSD) of the magnetic field in dB above a background averaged over the surrounding three minutes of each spectrum. The black lines mark $0.1f_{ce}$ and $0.3f_{ce}$; they are Gaussian smoothed with a standard deviation of 1 s in order to avoid obscuring the spectra. Panel (d): The PSD of the electric field normalized in the same manner as the \vec{B} PSD. This normalization diminishes continuous electrostatic power in the magnetosheath that extends from DC to the 150 Hz Nyquist frequency. These broadband emissions and the more narrowband electromagnetic power in panels (c) and (d) likely both contributed to the 100 Hz electric activity reported in (Scarf et al., 1980). Panel (e): the electron density moment. The time resolution is about one measurement every 28 seconds; data gaps are present in regions of high moment uncertainty.

121 Whistler emissions during PSP’s flyby of Venus began roughly a minute prior to
 122 the first bow shock crossing, which corresponds to a displacement of $0.24 r_v$ in the anti-
 123 sunward direction and $0.13 r_v$ in the dawn direction, where r_v is the radius of Venus. At
 124 low frequencies, both \vec{E} and \vec{B} feature erratic fluctuations with spectral peaks near 1 Hz.
 125 The wave amplitude ΔB is 1-2 nT in a 6 nT background field, and MVA over single wave

126 cycles shows circular polarization of \vec{B} with $\theta_{\pm\vec{k}-\vec{B}_0} \sim 30^\circ$. 1 Hz whistlers have been
 127 detected before in the upstream regions of Venus (Orlowski & Russell, 1991; Xiao et al.,
 128 2020), Mars (Brain et al., 2002), and Earth (e.g. Fairfield, 1974), almost exclusively in
 129 areas magnetically connected to the shock. We observe them to be strongest directly ad-
 130 jacent to the shock, which is consistent with prior observations, and suggests that they
 131 are generated here and damp out as they propagate upstream.

132 Figure 1 shows that this upstream region also contains higher frequency whistlers
 133 ($0.1f_{ce} < f < 0.3f_{ce}$), which have amplitudes near 0.15 nT and propagate parallel to
 134 \vec{B}_0 . Again, similar waves have been previously seen at Earth, both in the free solar wind
 135 and electron foreshock, and could indicate the presence of an upstream traveling elec-
 136 tron beam that excites a cyclotron resonance (Olson et al., 1969; Y. Zhang et al., 1998).

137 We focus on the upstream-to-downstream bow shock crossings at 08:22:30 and 08:29:00
 138 (labeled 1 and 3 above Figure 1.b), which occurred 3 - 4 r_v anti-sunward of Venus and
 139 together contain a representative sample of whistler waves. Upstream pointing shock nor-
 140 mal vectors \hat{n} were found by applying magnetic field coplanarity (Paschmann & Daly,
 141 1998). They suggest shock normal angles $\theta_{\hat{n}-\vec{B}_{0,up}}$ in the ranges of $20^\circ-40^\circ$ and $10^\circ-$
 142 20° for the 08:22:30 and 08:29:00 shocks, respectively. In the same order, the Alfvén Mach
 143 numbers of these shocks are about 6 and 8.

144 Figure 2 shows whistler waves at multiple frequencies during the bow shock cross-
 145 ing at 08:29. The hodograms of the wave in Figure 2, region (a) (hereafter referred to
 146 as region 2.a) are bandpass filtered between 20 and 40 Hz. The \vec{B} field hodogram is in
 147 the minimum variance plane, and shows coherent circular polarization. The propagation
 148 angle relative to the magnetic field $\theta_{\pm\vec{k}-\vec{B}_0}$ here is about 24° .

149 The orange ellipse in the \vec{E} hodogram is the projection of a circle around \vec{B}_0 into
 150 the \vec{E} field measurement plane. The size of the circle has been chosen to allow compar-
 151 ison with the data, and is not otherwise motivated. Although the \vec{E} field is not as co-
 152 herent as the \vec{B} field, it approximately traces out the orange ellipse over two of the three
 153 wave cycles plotted, as expected for a quasi-parallel whistler wave.

154 Their hodograms are not presented, but the waves around 08:29:05.0 are similar,
 155 propagating 20° from \vec{B}_0 at frequencies near 30 Hz. Both of these example waves are
 156 segments of $0.1f_{ce} < f < 0.3f_{ce}$ fluctuation power that grows out of minima in $|B_0|$
 157 and subsequently decays. The events begin with low frequency waves of the type in re-
 158 gion 2.b, and higher frequency waves grow as $|B_0|$ increases. A similar pattern is seen
 159 from 08:29:05.5 to 08:29:05.8, although the $|B_0|$ trough is substantially shallower here,
 160 and the subsequent waves (e.g. in region 2.c) decay more quickly.

161 Interacting whistler waves at different frequencies have also been observed in Earth's
 162 bow shock (Hull et al., 2012, 2020). A band with $f \sim 0.1 - 0.5f_{ce}$ and $\Delta B/|B_0| \sim$
 163 0.01 propagates quasi-parallel to \vec{B}_0 and is excited by lower frequency whistlers. The small
 164 amplitude waves in regions 2.a and 2.c may be representatives of an analogous band at
 165 Venus. At Earth, the low frequency waves are in the range of the lower hybrid frequency
 166 (f_{lh}) and propagate oblique to \vec{B}_0 with $\Delta B/|B_0| \sim 0.1-1$ (Hull et al., 2020). The rel-
 167 atively large amplitude whistlers in Figure 2 (e.g. in region 2.b, where $\Delta B/|B_0| \sim 0.06$)
 168 also propagate oblique to \vec{B}_0 and have frequencies similar to the mean of value of f_{lh} ,
 169 ~ 5 Hz, in the time span shown.

170 The region 2.b hodograms are bandpass filtered between 8 and 12 Hz. In $\beta \gtrsim 0.1$
 171 conditions, oblique whistler waves should have elliptical polarization of \vec{B} (Verkhoglyadova
 172 et al., 2013; Remya et al., 2016). In region 2.b, $\beta > 1$, so the approximately circular
 173 polarization here is surprising. Still, it is clear that \vec{E} and \vec{B} are coupled and constitute
 174 an electromagnetic wave – their cross coherence is approximately 1 in a 4 Hz-wide band

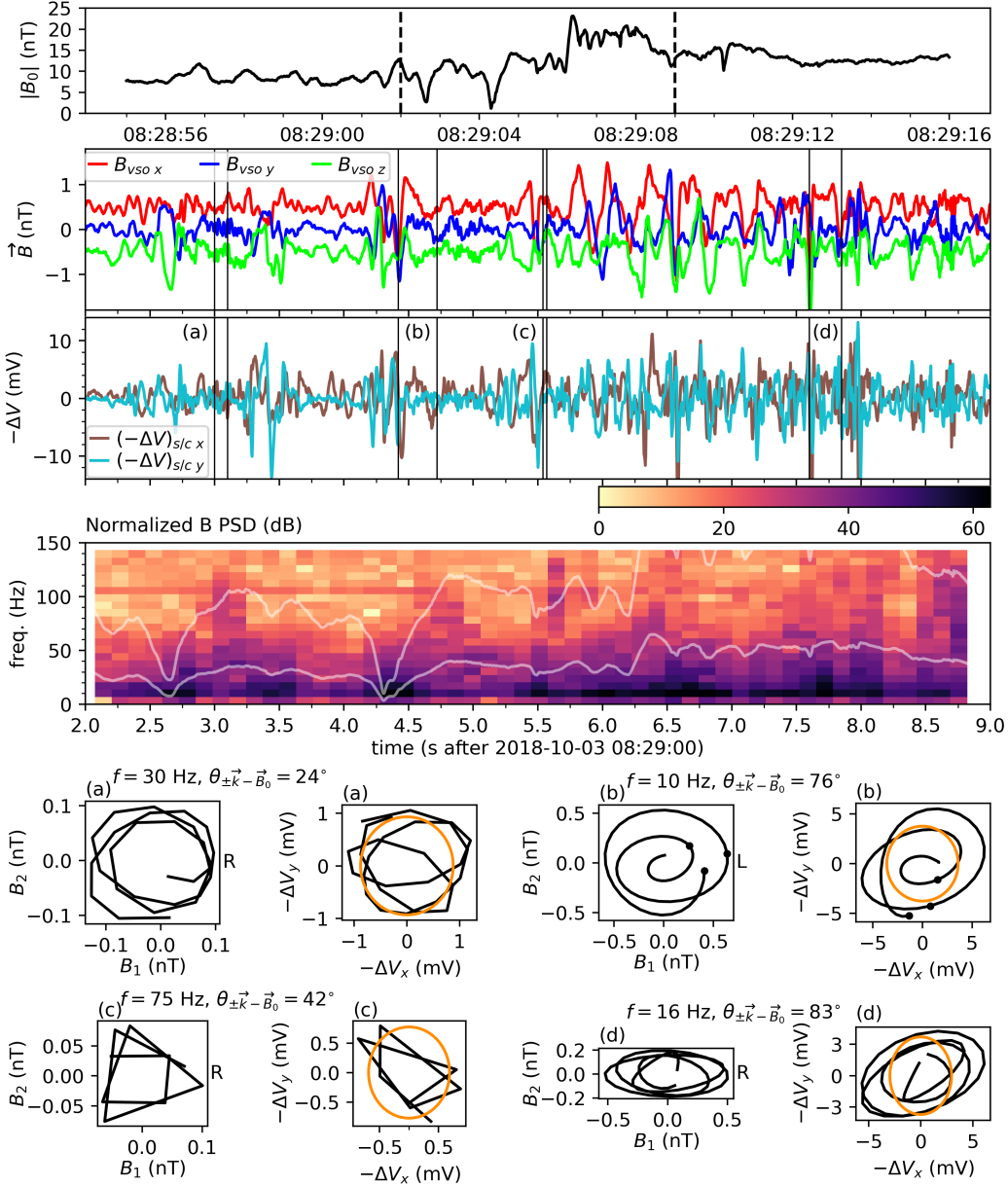


Figure 2. Whistler waves at multiple scales within the bow shock. The top panel shows an overview of the magnetic field magnitude. The vertical dashed black lines mark the time limits of the next three panels. Panels 2 and 3 show magnetic field in VSO coordinates and electric field in spacecraft coordinates; both are high-pass filtered above 4 Hz. We plot the potential differences measured by the antennas instead of the electric field due to lack of knowledge of the effective antenna lengths during this time. For each of the regions labeled (a), (b), (c), and (d), there are two hodograms: one of \vec{B} and one of \vec{E} . The \vec{B} field hodogram is in the minimum variance plane. The \vec{E} field hodogram is in the spacecraft X-Y plane. The orange trace is the projection of a circle around \vec{B}_0 into the \vec{E} field measurement plane. To the right of each \vec{B} hodogram, either R or L is written, which stand for right- or left-handed rotation of \vec{B} about \vec{B}_0 . The appearance of left-handed polarization for the region (b) wave is addressed in Section 4.3.

175 centered at 10 Hz. Black dots have been added to their hodograms at three equally spaced
 176 positions starting at $t = 0$. The fields both spiral inwards as the wave decays.

177 **4 $f < 0.1f_{ce}$ Whistler Waves Propagating $> 80^\circ$ Oblique to \vec{B}_0**

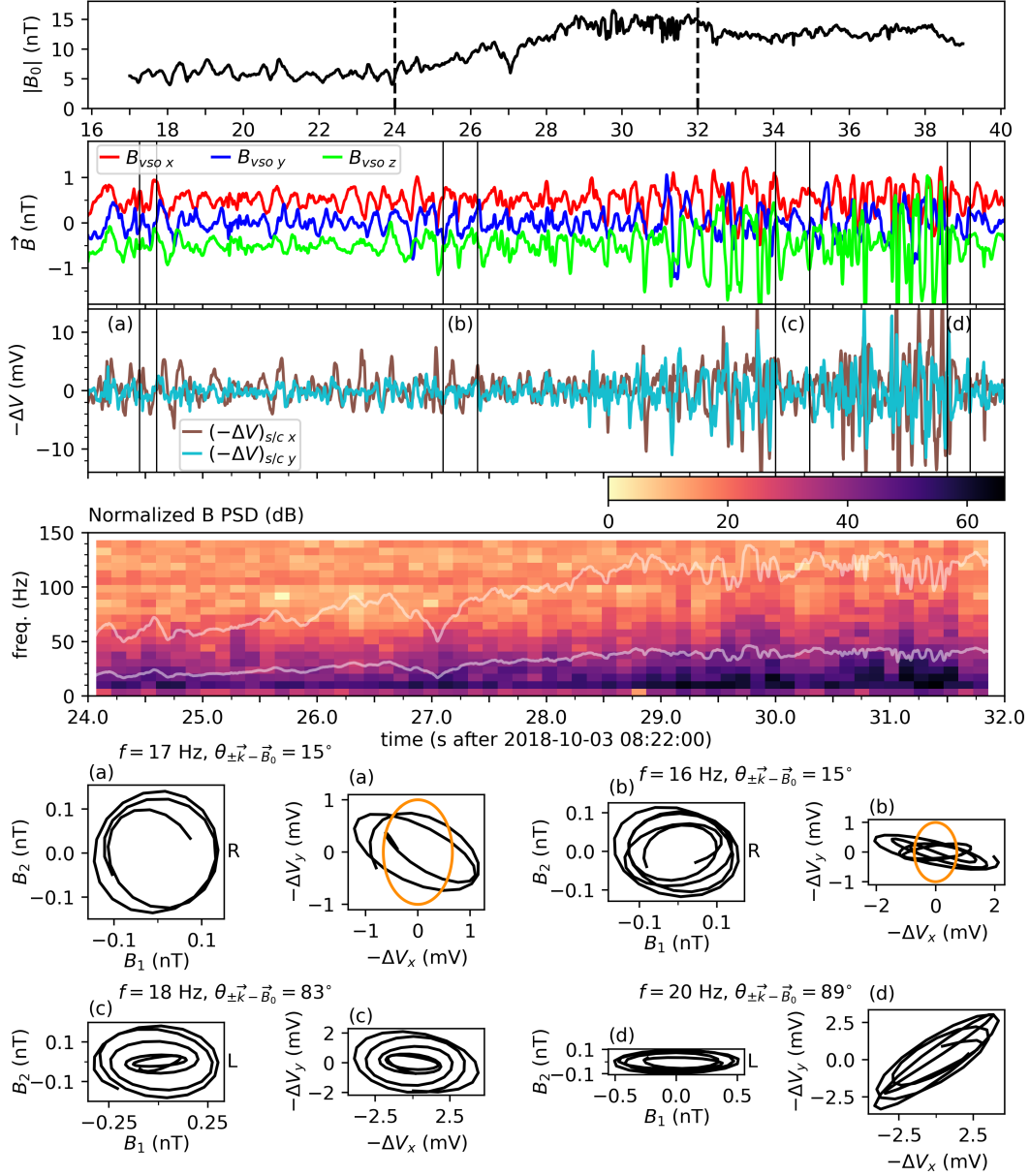


Figure 3. Low frequency whistler waves in the magnetic ramp of the 08:22:30 bow shock crossing. For the quasi-parallel propagating waves in regions (a) and (b), disagreement between the electric field hodograms and the orange ellipse is unexpected, and may be caused by instrumental distortion of the \vec{E} field. The elliptical polarization of \vec{B} seen for the oblique waves in regions (c) and (d) is expected in warm plasmas. These waves have left-handed polarization about \vec{B}_0 in the spacecraft frame, which is discussed in Section 4.3 and is likely due to Doppler shifting.

178

4.1 Polarization of \vec{B}

179

180

181

182

183

184

185

186

The 08:22:30 bow shock crossing is presented in Figure 3. Downstream of the \vec{B}_0 shock discontinuities, the 08:22:30 and 08:29:00 crossings both feature very oblique waves, examples of which are in regions 2.d, 3.c, and 3.d. To isolate these waves from the broadband low frequency spectrum, 2nd order Butterworth filters with 4 Hz-wide passbands were applied to the data. The resulting waveforms have elliptically polarized \vec{B} , in agreement with predictions by Verkhoglyadova et al. (2013) for oblique whistlers in warm plasmas. In cold plasmas, \vec{B} is circularly polarized regardless of the propagation angle $\theta_{\vec{k}-\vec{B}_0}$; the observed ellipticity is caused by thermal electron motion (Verkhoglyadova et al., 2010).

187

188

189

190

We denote the maximum and intermediate variance directions determined by MVA as $\hat{e}_{MVA\ B,1}$ and $\hat{e}_{MVA\ B,2}$, respectively. \hat{z}' is defined as the direction (either \hat{k} or $-\hat{k}$) around which \vec{B} rotates in a right-handed sense. Following Verkhoglyadova et al. (2010), we also define \hat{y} as a unit vector in the $\vec{B}_0 \times \hat{z}'$ direction and $\hat{x}' = \hat{y} \times \hat{z}'$.

191

192

193

194

As illustrated in Figure 4, \vec{B} 's semimajor axis should lie in the \hat{x}' direction and its semiminor axis should lie in the \hat{y} direction (Verkhoglyadova et al., 2013; Remya et al., 2016). We find in each of the regions 2.d, 3.c, and 3.d, $|\hat{e}_{MVA\ B,2} \cdot \hat{y}| > 0.98$, confirming theoretical predictions. $|\hat{e}_{MVA\ B,1} \cdot \hat{x}'| \sim 1$ naturally follows.

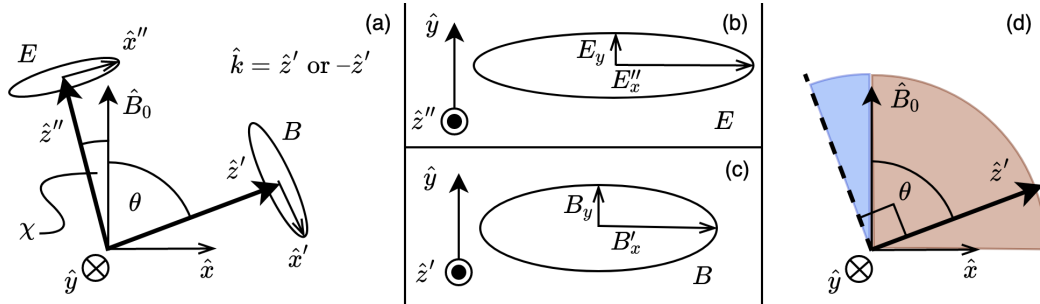


Figure 4. Polarization of oblique whistler waves. Panel (a) demonstrates that \vec{B}_0 , the polarization axis of \vec{E} (\hat{z}''), and the polarization axis of \vec{B} (\hat{z}') are co-planar. Here \hat{z}' and \hat{z}'' are defined to be the directions around which \vec{B} and \vec{E} rotate in a right-handed sense. Equation 1 provides a relationship between \vec{B} ellipticity, \vec{E} ellipticity, and $\theta + \chi$. For the wave illustrated, this is satisfied by $|B_y/B'_x| \approx 1/2.75$, $|E''_x/E_y| \approx 4.25$, and $\theta + \chi \approx 85^\circ$. For the direction of \hat{z}' shown, the blue and brown shadings in panel (d) mark allowed orientations for \hat{z}'' under various assumptions – the brown sector may not be allowed. See the text for details.

195

4.2 Polarization of \vec{E}

196

197

198

199

200

Kinetic theory and Maxwell's equations make predictions for the electric field polarization that we did not observe, most likely due to instrumental effects. For the following, \hat{z}' is again the axis around which \vec{B} rotates in a right-handed sense, and θ is its inclination from \vec{B}_0 . \hat{z}'' is the axis around which \vec{E} rotates in a right-handed sense, and χ is its inclination from \vec{B}_0 .

201

202

203

204

205

206

For plasma with an electron velocity distribution function of the form $f(v_\perp^2, v_\parallel)$ in a uniform background \vec{B}_0 , \hat{z}'' is coplanar with \hat{k} and \hat{B}_0 (Krall & Trivelpiece, 1973; Verkhoglyadova et al., 2013). In addition, from Faraday's law, \vec{E} and \vec{B} must rotate in the same sense about \hat{k} , restricting \hat{z}'' to lie within 90° of \hat{z}' . To produce whistler mode electron dynamics, \vec{E} must also rotate in a right-handed sense about \hat{B}_0 , likewise restricting \hat{z}'' to lie within 90° of \hat{B}_0 (Jackson, 1999).

207 In full, these criteria limit \hat{z}'' to a $(180^\circ - \theta)$ span in the $\hat{B}_0 - \hat{z}'$ plane. This win-
 208 dows is marked by the union of the blue and brown sectors in Figure 4.d. In the cold plasma
 209 approximation, Verkhoglyadova et al. (2010) show that \hat{z}' and \hat{z}'' are canted to oppo-
 210 site directions with respect to \vec{B}_0 , so both θ and χ as illustrated in Figure 4.a are pos-
 211 itive, and \hat{z}'' is limited to the blue sector in Figure 4.d. For the region 2.d, 3.c, and 3.d
 212 waves, $\theta_{\pm\vec{k}-\vec{B}_0} > 80^\circ$ with the restrictions $\chi > 0^\circ$ and $\chi + \theta < 90^\circ$ leaves a window
 213 for χ smaller than 10° .

214 Faraday's law also gives information about the ellipticities of \vec{E} and \vec{B} – in the plane
 215 perpendicular to \hat{k} , they are equal: $|E'_x/E'_y| = |B_y/B'_x|$ (Bellan, 2013). This provides a
 216 relationship between \vec{B} ellipticity, \vec{E} ellipticity, and the angle of inclination, $\theta + \chi$, be-
 217 tween the \vec{E} and \vec{B} polarization planes

$$\frac{E'_x}{E'_y} = \frac{E''_x \cos(\theta + \chi)}{E''_y} = \frac{B_y}{B'_x} \quad (1)$$

218 For each position of \hat{z}'' in the blue sector in Figure 4.d, Equation 1 was enforced, and
 219 the resulting \vec{E} ellipse was projected into the antenna measurement plane and compared
 220 with observations. For the waves in regions 2.d, 3.c, and 3.d, this search was unsuccess-
 221 ful.

222 Allowing for the possibility that the cold plasma stipulation $\chi > 0^\circ$ does not ex-
 223 tend to warm plasmas, the same procedure was applied for orientations of \hat{z}'' in the brown
 224 sector in Figure 4.d, but again agreement with the observed \vec{E} field was not found. This
 225 may point to the need for a low frequency correction to the ΔV measured by the anten-
 226 nas. This need is evident in the DC electric field measurements, which often diverge from
 227 $-\vec{v} \times \vec{B}$ (Mozer et al., 2020; Bowen et al., 2020).

228 Regions 3.a and 3.b also indicate that the measured \vec{E} field may be distorted by
 229 instrumental effects. These ~ 16 Hz waves propagate quasi-parallel to \vec{B}_0 and appropri-
 230 ately have circularly polarized \vec{B} . The divergences of the \vec{E} field hodograms from the
 231 orange ellipses indicate that the measured \vec{E} is not approximately circularly polarized
 232 around \vec{B}_0 , which it should be provided that these waves are whistlers.

233 4.3 Doppler Shifting and Wave Damping

234 The region 2.b, 3.c, and 3.d waves have left-handed polarization about \vec{B}_0 in the
 235 spacecraft frame, so if they are whistlers, a Doppler shift must have inverted their in-
 236 trinsic right-handed polarization. Alternatively, they could be ion-cyclotron waves (ICW).
 237 However, Krauss-Varban et al. (1994) show that the magnetic field of an oblique ICW
 238 is predominantly out of the $\vec{k} - \vec{B}_0$ plane, while for the region 3.c and 3.d waves, it is
 239 predominantly in this plane. This observed polarization conforms with the whistler branch
 240 in both the high frequency (Verkhoglyadova et al., 2013; Remya et al., 2016) and low fre-
 241 quency fast/magnetosonic regimes (Krauss-Varban et al., 1994).

242 Provided that the waves are whistlers, their plasma frame frequencies must lie be-
 243 low the resonance frequency $f_{ce} \cos(\theta_{\pm\vec{k}-\vec{B}_0})$, which is in the tens of Hz range. The ob-
 244 served 20 Hz left-handed rotation would then require a Doppler shift $\Delta f = |\hat{k} \cdot \vec{v}_{plasma}|/\lambda$
 245 in the range of 20–100 Hz. Here \vec{v}_{plasma} is the velocity of the plasma in the spacecraft
 246 frame, λ is the wavelength, and $\hat{k} \cdot \vec{v}_{plasma}$ must be negative to shift from right-handed
 247 to left-handed polarization. For these waves, $|\hat{k} \cdot \vec{v}| \sim 200$ km/s, giving wavelengths
 248 $\lambda \sim 2-10$ km. This is similar to the electron inertial length in this region: $k_\perp c/\omega_{pe} \sim$
 249 $0.6-3$, where k_\perp is the perpendicular wavenumber $(2\pi/\lambda) \sin(\theta_{\pm\vec{k}-\vec{B}_0})$ and ω_{pe} is the
 250 electron plasma frequency $\sqrt{n_e e^2/(m_e \epsilon_0)}$. In this regime, the waves undergo electron
 251 Landau damping, but at a rate that allows them to persist for several cycles (e.g. Gary
 252 & Smith, 2009).

253 The polarization of \vec{B} in the region 2.b wave is not unique to whistler waves or ion-
 254 cyclotron waves, so cannot be used to distinguish between modes. However, a different
 255 method can be used to rule out the ICW. The wave's spacecraft frame frequency, $f_{sc} = 10$
 256 Hz, is much larger than the ion-cyclotron frequency, so if the wave is an ICW, f_{sc} is al-
 257 most entirely due to Doppler shifting: $f_{sc} \approx \vec{k} \cdot \vec{v}_{plasma} / \lambda$. This gives a wavelength of
 258 about 20 km, which is much smaller than the ion inertial length: $k_{\perp} c / \omega_{pi} \sim 13$. Gary
 259 and Smith (2009) show that this results in a damping rate that is much faster than the
 260 wave frequency, preventing propagation.

261 5 Conclusions

262 Whistlers are a prominent feature of the low frequency dynamics in the Venusian
 263 bow shock. In the shock transition region, waves with $f \lesssim 0.1 f_{ce}$ preferentially grow
 264 out of minima in $|B_0|$, and can be oblique (2.b) or parallel-propagating (3.b). Higher fre-
 265 quency waves with $0.1 f_{ce} < f < 0.4 f_{ce}$ (2.a, 2.c) are strongest in the downstream ramps
 266 of these $|B_0|$ minima.

267 Bandpass filtering the erratic electric and magnetic fields downstream of the shock
 268 discontinuity in \vec{B}_0 reveals oblique, elliptically polarized whistlers (2.d, 3.c, 3.d). The
 269 orientations of the semiminor and semimajor axes of these waves' \vec{B} field ellipses are found
 270 to agree with predictions from kinetic theory to high accuracy. This demonstrates that
 271 thermal electron motion can have a pronounced effect on whistler wave polarization in
 272 plasmas accessible to spacecraft.

273 The same waves may also be present downstream of Earth's bow shock. Here, MMS
 274 measures 3D electric and magnetic fields, so the polarization properties of these waves
 275 could be examined in more detail (Burch et al., 2016). If sufficiently well understood,
 276 the waves could serve as a window into thermal electron motion in the turbulent plasma
 277 downstream of magnetized collisionless shocks.

Acknowledgments

The FIELDS and SWEAP instruments on the Parker Solar Probe spacecraft were designed and developed under NASA contract NNN06AA01C. Data from these instruments are publicly available:

FIELDS: <https://fields.ssl.berkeley.edu/data/>

SWEAP: <http://sweap.cfa.harvard.edu/Data.html>

References

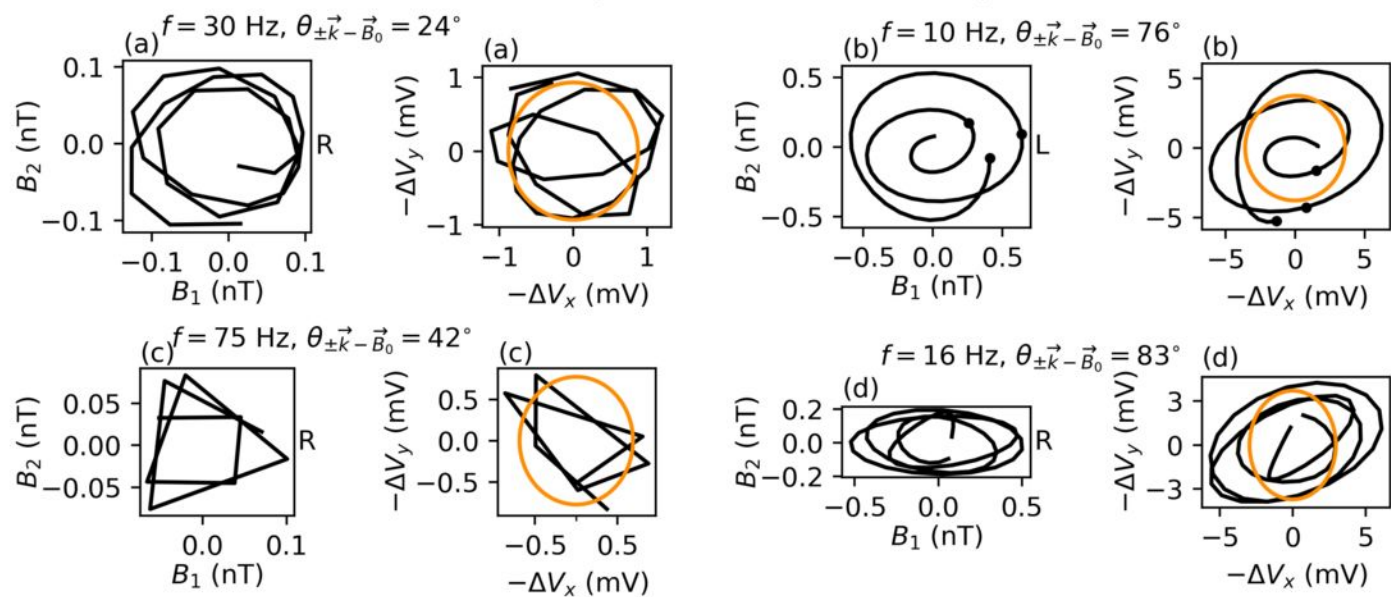
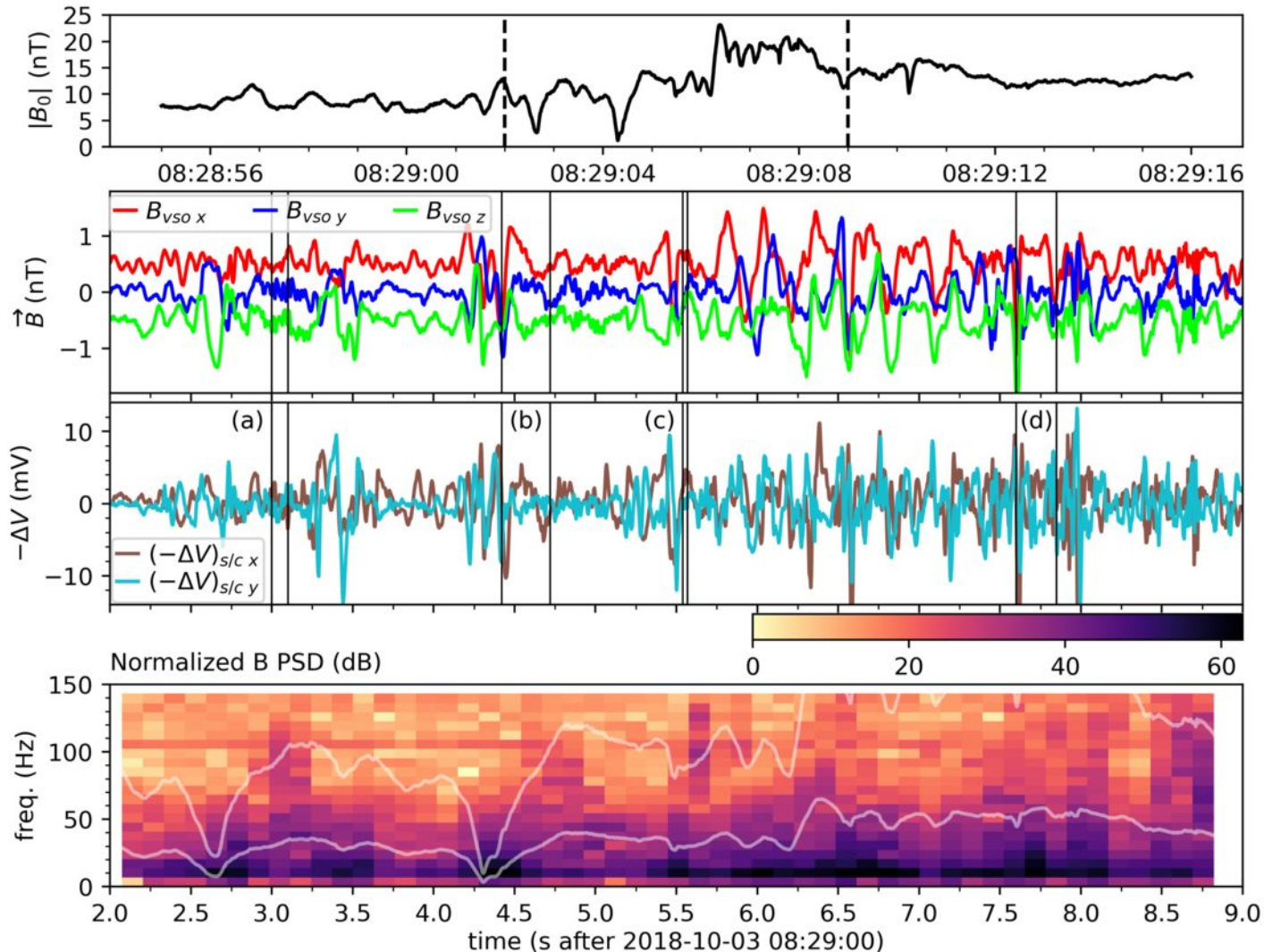
- Bale, S. D., Goetz, K., Harvey, P. R., Turin, P., Bonnell, J. W., Dudok de Wit, T., ... Wygant, J. R. (2016, Dec 01). The fields instrument suite for solar probe plus. *Space Science Reviews*, *204*(1), 49-82. Retrieved from <https://doi.org/10.1007/s11214-016-0244-5> doi: 10.1007/s11214-016-0244-5
- Bellan, P. M. (2013). Circular polarization of obliquely propagating whistler wave magnetic field. *Physics of Plasmas*, *20*(8), 082113. Retrieved from <https://doi.org/10.1063/1.4817964> doi: 10.1063/1.4817964
- Bowen, T. A., Bale, S. D., Bonnell, J., Larson, D., Mallet, A., McManus, M. D., ... Psp/Sweap Teams (2020, Aug). The Electromagnetic Signature of Outward Propagating Ion-scale Waves. *The Astrophysical Journal*, *899*(1), 74. doi: 10.3847/1538-4357/ab9f37
- Bowen, T. A., Bale, S. D., Bonnell, J. W., Dudok de Wit, T., Goetz, K., Goodrich, K., ... Szabo, A. (2020). A merged search-coil and fluxgate magnetometer data product for parker solar probe fields. *Journal of Geophysical Research: Space Physics*, *125*(5), e2020JA027813. Retrieved from <https://agupubs.onlinelibrary.wiley.com/doi/abs/10.1029/2020JA027813> (e2020JA027813 10.1029/2020JA027813) doi: 10.1029/2020JA027813
- Brain, D. A., Bagenal, F., AcuAa, M. H., Connerney, J. E. P., Crider, D. H., Mazelle, C., ... Ness, N. F. (2002). Observations of low-frequency electromagnetic plasma waves upstream from the martian shock. *Journal of Geophysical Research: Space Physics*, *107*(A6), SMP 9-1-SMP 9-11. Retrieved from <https://agupubs.onlinelibrary.wiley.com/doi/abs/10.1029/2000JA000416> doi: 10.1029/2000JA000416
- Burch, J. L., Moore, T. E., Torbert, R. B., & Giles, B. L. (2016). Magnetospheric multiscale overview and science objectives. *Space Science Reviews*, *199*(1-4), 5-21. doi: 10.1007/s11214-015-0164-9
- Case, A. W., Kasper, J. C., Stevens, M. L., Korreck, K. E., Paulson, K., Daigneau, P., ... Martinović, M. M. (2020, feb). The solar probe cup on the parker solar probe. *The Astrophysical Journal Supplement Series*, *246*(2), 43. Retrieved from <https://doi.org/10.3847/2F1538-4365%2Fab5a7b> doi: 10.3847/1538-4365/ab5a7b
- Fairfield, D. H. (1974). Whistler waves observed upstream from collisionless shocks. *Journal of Geophysical Research (1896-1977)*, *79*(10), 1368-1378. Retrieved from <https://agupubs.onlinelibrary.wiley.com/doi/abs/10.1029/JA079i010p01368> doi: 10.1029/JA079i010p01368
- Gary, S. P., & Smith, C. W. (2009). Short-wavelength turbulence in the solar wind: Linear theory of whistler and kinetic alfvén fluctuations. *Journal of Geophysical Research: Space Physics*, *114*(A12). Retrieved from <https://agupubs.onlinelibrary.wiley.com/doi/abs/10.1029/2009JA014525> doi: 10.1029/2009JA014525
- Holzer, R. E., Northrop, T. G., Olson, J. V., & Russell, C. T. (1972). Study of waves in the earth's bow shock. *Journal of Geophysical Research (1896-1977)*, *77*(13), 2264-2273. Retrieved from <https://agupubs.onlinelibrary.wiley.com/doi/abs/10.1029/JA077i013p02264> doi: 10.1029/JA077i013p02264
- Hull, A. J., Muschietti, L., Le Contel, O., Dorelli, J. C., & Lindqvist, P.-A. (2020).

- 330 Mms observations of intense whistler waves within earth's supercritical bow
 331 shock: Source mechanism and impact on shock structure and plasma trans-
 332 port. *Journal of Geophysical Research: Space Physics*, 125(7), e2019JA027290.
 333 Retrieved from [https://agupubs.onlinelibrary.wiley.com/doi/abs/](https://agupubs.onlinelibrary.wiley.com/doi/abs/10.1029/2019JA027290)
 334 10.1029/2019JA027290 (e2019JA027290 10.1029/2019JA027290) doi:
 335 10.1029/2019JA027290
- 336 Hull, A. J., Muschietti, L., Oka, M., Larson, D. E., Mozer, F. S., Chaston, C. C.,
 337 ... Hospodarsky, G. B. (2012). Multiscale whistler waves within earth's
 338 perpendicular bow shock. *Journal of Geophysical Research: Space Physics*,
 339 117(A12). Retrieved from [https://agupubs.onlinelibrary.wiley.com/](https://agupubs.onlinelibrary.wiley.com/doi/abs/10.1029/2012JA017870)
 340 doi/abs/10.1029/2012JA017870 doi: 10.1029/2012JA017870
- 341 Jackson, J. D. (1999). Classical electrodynamics. In (3rd ed. ed., p. 316-317). New
 342 York, NY: Wiley.
- 343 Kasper, J. C., Abiad, R., Austin, G., Balat-Pichelin, M., Bale, S. D., Belcher, J. W.,
 344 ... others (2016). Solar wind electrons alphas and protons (sweap) investi-
 345 gation: design of the solar wind and coronal plasma instrument suite for solar
 346 probe plus. *Space Science Reviews*, 204(1-4), 131-186.
- 347 Krall, N. A., & Trivelpiece, A. W. (1973). Principles of plasma physics. krall. In
 348 (p. 402-407). New York: McGraw-Hill.
- 349 Krauss-Varban, D., Omidi, N., & Quest, K. B. (1994). Mode properties of
 350 low-frequency waves: Kinetic theory versus hall-mhd. *Journal of Geo-*
 351 *physical Research: Space Physics*, 99(A4), 5987-6009. Retrieved from
 352 <https://agupubs.onlinelibrary.wiley.com/doi/abs/10.1029/93JA03202>
 353 doi: 10.1029/93JA03202
- 354 Malaspina, D. M., Ergun, R. E., Bolton, M., Kien, M., Summers, D., Stevens, K., ...
 355 Goetz, K. (2016). The digital fields board for the fields instrument suite on the
 356 solar probe plus mission: Analog and digital signal processing. *Journal of Geo-*
 357 *physical Research: Space Physics*, 121(6), 5088-5096. Retrieved from [https://](https://agupubs.onlinelibrary.wiley.com/doi/abs/10.1002/2016JA022344)
 358 agupubs.onlinelibrary.wiley.com/doi/abs/10.1002/2016JA022344 doi:
 359 10.1002/2016JA022344
- 360 Mozer, F. S., Agapitov, O. V., Bale, S. D., Bonnell, J. W., Bowen, T. A., & Vasko,
 361 I. (2020). Dc and low-frequency electric field measurements on the parker
 362 solar probe. *Journal of Geophysical Research: Space Physics*, 125(9),
 363 e2020JA027980. Retrieved from [https://agupubs.onlinelibrary.wiley](https://agupubs.onlinelibrary.wiley.com/doi/abs/10.1029/2020JA027980)
 364 [.com/doi/abs/10.1029/2020JA027980](https://agupubs.onlinelibrary.wiley.com/doi/abs/10.1029/2020JA027980) (e2020JA027980 2020JA027980) doi:
 365 10.1029/2020JA027980
- 366 Oka, M., III, L. B. W., Phan, T. D., Hull, A. J., Amano, T., Hoshino, M., ...
 367 Lindqvist, P. A. (2017, jun). Electron scattering by high-frequency whistler
 368 waves at earth's bow shock. *The Astrophysical Journal*, 842(2), L11. Re-
 369 trieved from <https://doi.org/10.3847/2041-8213/aa7759> doi:
 370 10.3847/2041-8213/aa7759
- 371 Oka, M., Otsuka, F., Matsukiyo, S., Wilson, L. B., Argall, M. R., Amano, T., ...
 372 Lindqvist, P. A. (2019, nov). Electron scattering by low-frequency whistler
 373 waves at earth's bow shock. *The Astrophysical Journal*, 886(1), 53. Re-
 374 trieved from <https://doi.org/10.3847/201538-4357/ab4a81> doi:
 375 10.3847/1538-4357/ab4a81
- 376 Olson, J. V., Holzer, R. E., & Smith, E. J. (1969). High-frequency magnetic
 377 fluctuations associated with the earth's bow shock. *Journal of Geophys-*
 378 *ical Research (1896-1977)*, 74(19), 4601-4617. Retrieved from [https://](https://agupubs.onlinelibrary.wiley.com/doi/abs/10.1029/JA074i019p04601)
 379 agupubs.onlinelibrary.wiley.com/doi/abs/10.1029/JA074i019p04601
 380 doi: 10.1029/JA074i019p04601
- 381 Orłowski, D. S., & Russell, C. T. (1991). Ulf waves upstream of the venus
 382 bow shock: Properties of one-hertz waves. *Journal of Geophysical Re-*
 383 *search: Space Physics*, 96(A7), 11271-11282. Retrieved from [https://](https://agupubs.onlinelibrary.wiley.com/doi/abs/10.1029/91JA01103)
 384 agupubs.onlinelibrary.wiley.com/doi/abs/10.1029/91JA01103 doi:

- 10.1029/91JA01103
- 385 Paschmann, G., & Daly, P. W. (1998, January). Analysis Methods for Multi-
 386 Spacecraft Data. ISSI Scientific Reports Series SR-001, ESA/ISSI, Vol. 1.
 387 ISBN 1608-280X, 1998. *ISSI Scientific Reports Series, 1*.
- 388 Remya, B., Lee, K. H., Lee, L. C., & Tsurutani, B. T. (2016). Polarization of
 389 obliquely propagating whistler mode waves based on linear dispersion the-
 390 ory. *Physics of Plasmas, 23*(12), 122120. Retrieved from [https://doi.org/](https://doi.org/10.1063/1.4972534)
 391 [10.1063/1.4972534](https://doi.org/10.1063/1.4972534) doi: 10.1063/1.4972534
- 392 Rodriguez, P., & Gurnett, D. A. (1975). Electrostatic and electromagnetic tur-
 393 bulence associated with the earth's bow shock. *Journal of Geophysical*
 394 *Research (1896-1977), 80*(1), 19-31. Retrieved from [https://agupubs](https://agupubs.onlinelibrary.wiley.com/doi/abs/10.1029/JA080i001p00019)
 395 [.onlinelibrary.wiley.com/doi/abs/10.1029/JA080i001p00019](https://agupubs.onlinelibrary.wiley.com/doi/abs/10.1029/JA080i001p00019) doi:
 396 [10.1029/JA080i001p00019](https://agupubs.onlinelibrary.wiley.com/doi/abs/10.1029/JA080i001p00019)
- 397 Scarf, F. L., Taylor, W. W. L., Russell, C. T., & Elphic, R. C. (1980). Pioneer
 398 venus plasma wave observations: The solar wind-venus interaction. *Jour-*
 399 *nal of Geophysical Research: Space Physics, 85*(A13), 7599-7612. Retrieved
 400 from [https://agupubs.onlinelibrary.wiley.com/doi/abs/10.1029/](https://agupubs.onlinelibrary.wiley.com/doi/abs/10.1029/JA085iA13p07599)
 401 [JA085iA13p07599](https://agupubs.onlinelibrary.wiley.com/doi/abs/10.1029/JA085iA13p07599) doi: 10.1029/JA085iA13p07599
- 402 Sonnerup, B. U., & Scheible, M. (1998). Minimum and maximum variance analysis.
 403 *Analysis methods for multi-spacecraft data, 185–220*.
- 404 Strangeway, R. J., & Crawford, G. K. (1993). On the instability and energy flux of
 405 lower hybrid waves in the venus plasma mantle. *Geophysical Research Letters,*
 406 *20*(12), 1211-1214. Retrieved from [https://agupubs.onlinelibrary.wiley](https://agupubs.onlinelibrary.wiley.com/doi/abs/10.1029/93GL01354)
 407 [.com/doi/abs/10.1029/93GL01354](https://agupubs.onlinelibrary.wiley.com/doi/abs/10.1029/93GL01354) doi: 10.1029/93GL01354
- 408 Szegő, K., Shapiro, V. S., Shevchenko, V. I., Sagdeev, R. Z., Kasprzak, W. T.,
 409 & Nagy, A. F. (1991). Physical processes in the plasma mantle of
 410 venus. *Geophysical Research Letters, 18*(12), 2305-2308. Retrieved from
 411 <https://agupubs.onlinelibrary.wiley.com/doi/abs/10.1029/91GL02086>
 412 [doi: 10.1029/91GL02086](https://agupubs.onlinelibrary.wiley.com/doi/abs/10.1029/91GL02086)
- 413 Verkhoglyadova, O. P., Tsurutani, B. T., & Lakhina, G. S. (2010). Properties of
 414 obliquely propagating chorus. *Journal of Geophysical Research: Space Physics,*
 415 *115*(A9). Retrieved from [https://agupubs.onlinelibrary.wiley.com/doi/](https://agupubs.onlinelibrary.wiley.com/doi/abs/10.1029/2009JA014809)
 416 [abs/10.1029/2009JA014809](https://agupubs.onlinelibrary.wiley.com/doi/abs/10.1029/2009JA014809) doi: 10.1029/2009JA014809
- 417 Verkhoglyadova, O. P., Tsurutani, B. T., & Lakhina, G. S. (2013). Theoretical
 418 analysis of poynting flux and polarization for elf-vlf electromagnetic waves in
 419 the earth's magnetosphere. *Journal of Geophysical Research: Space Physics,*
 420 *118*(12), 7695-7702. Retrieved from [https://agupubs.onlinelibrary.wiley](https://agupubs.onlinelibrary.wiley.com/doi/abs/10.1002/2013JA019371)
 421 [.com/doi/abs/10.1002/2013JA019371](https://agupubs.onlinelibrary.wiley.com/doi/abs/10.1002/2013JA019371) doi: 10.1002/2013JA019371
- 422 Whittlesey, P. L., Larson, D. E., Kasper, J. C., Halekas, J., Abatcha, M., Abiad,
 423 R., ... Verniero, J. L. (2020, mar). The solar probe ANalyzers—electrons on
 424 the parker solar probe. *The Astrophysical Journal Supplement Series, 246*(2),
 425 74. Retrieved from <https://doi.org/10.3847/1538-4365/ab7370> doi:
 426 [10.3847/1538-4365/ab7370](https://doi.org/10.3847/1538-4365/ab7370)
- 427 Wilson III, L. B., Sibeck, D. G., Breneman, A. W., Contel, O. L., Cully, C., Turner,
 428 D. L., ... Malaspina, D. M. (2014). Quantified energy dissipation rates in
 429 the terrestrial bow shock: 2. waves and dissipation. *Journal of Geophysi-*
 430 *cal Research: Space Physics, 119*(8), 6475-6495. Retrieved from [https://](https://agupubs.onlinelibrary.wiley.com/doi/abs/10.1002/2014JA019930)
 431 agupubs.onlinelibrary.wiley.com/doi/abs/10.1002/2014JA019930 doi:
 432 [10.1002/2014JA019930](https://agupubs.onlinelibrary.wiley.com/doi/abs/10.1002/2014JA019930)
- 433 Xiao, S., Wu, M., Wang, G., Chen, Y., & Zhang, T. (2020). Survey of 1-hz waves
 434 in the near-venusian space: Venus express observations. *Planetary and Space*
 435 *Science, 187,* 104933. Retrieved from [http://www.sciencedirect.com/](http://www.sciencedirect.com/science/article/pii/S0032063320300532)
 436 [science/article/pii/S0032063320300532](http://www.sciencedirect.com/science/article/pii/S0032063320300532) doi: [https://doi.org/10.1016/](https://doi.org/10.1016/j.pss.2020.104933)
 437 [j.pss.2020.104933](https://doi.org/10.1016/j.pss.2020.104933)
- 438 Zhang, T., Delva, M., Baumjohann, W., Volwerk, M., Russell, C., Barabash, S., ...

- 440 Zambelli, W. (2008). Initial venus express magnetic field observations of the
441 venus bow shock location at solar minimum. *Planetary and Space Science*,
442 *56*(6), 785 - 789. Retrieved from [http://www.sciencedirect.com/science/
443 article/pii/S0032063307003777](http://www.sciencedirect.com/science/article/pii/S0032063307003777) (Mars Express/Venus Express) doi:
444 <https://doi.org/10.1016/j.pss.2007.09.012>
- 445 Zhang, Y., Matsumoto, H., & Kojima, H. (1998). Bursts of whistler mode waves
446 in the upstream of the bow shock: Geotail observations. *Journal of Geophys-
447 ical Research: Space Physics*, *103*(A9), 20529-20540. Retrieved from [https://
448 agupubs.onlinelibrary.wiley.com/doi/abs/10.1029/98JA01371](https://agupubs.onlinelibrary.wiley.com/doi/abs/10.1029/98JA01371) doi: 10
449 .1029/98JA01371
- 450 Zhang, Y., Matsumoto, H., Kojima, H., & Omura, Y. (1999). Extremely in-
451 tense whistler mode waves near the bow shock: Geotail observations. *Jour-
452 nal of Geophysical Research: Space Physics*, *104*(A1), 449-461. Retrieved
453 from [https://agupubs.onlinelibrary.wiley.com/doi/abs/10.1029/
454 1998JA900049](https://agupubs.onlinelibrary.wiley.com/doi/abs/10.1029/1998JA900049) doi: 10.1029/1998JA900049

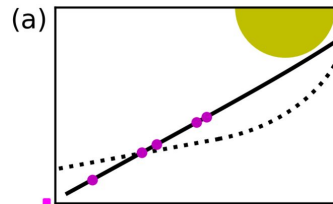
new_bs2_rev2.png.



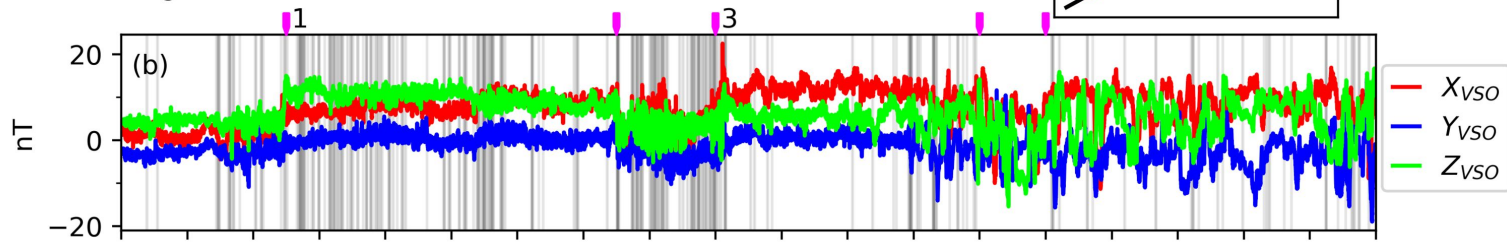
new_new_overview.png.

1: $\theta_{\hat{n} - \vec{B}_{0,up}} = 20^\circ - 40^\circ, M_A \approx 6$

3: $\theta_{\hat{n} - \vec{B}_{0,up}} = 10^\circ - 20^\circ, M_A \approx 8$

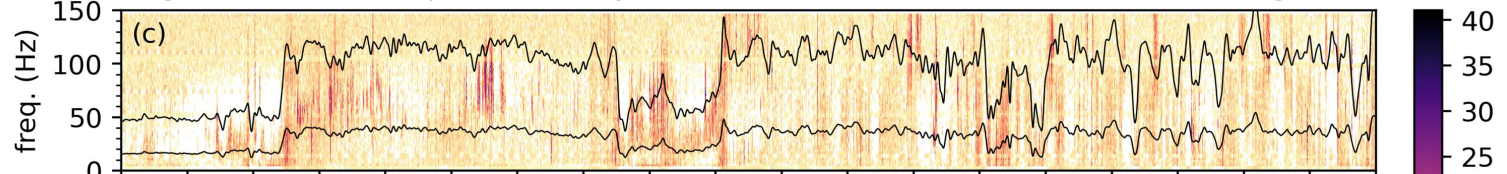


Magnetic Field Time Series



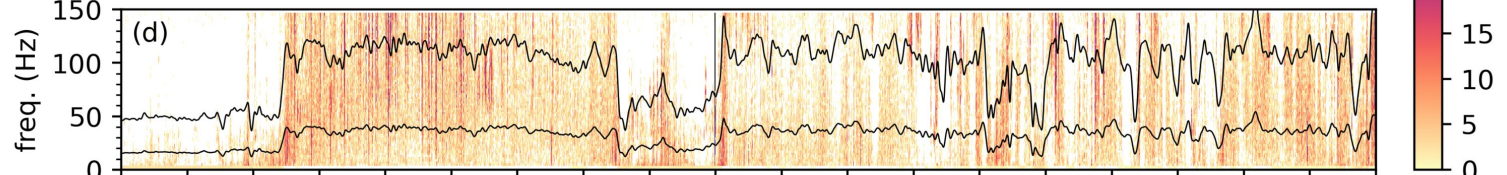
Magnetic Field Power Spectral Density

(dB Above Background)

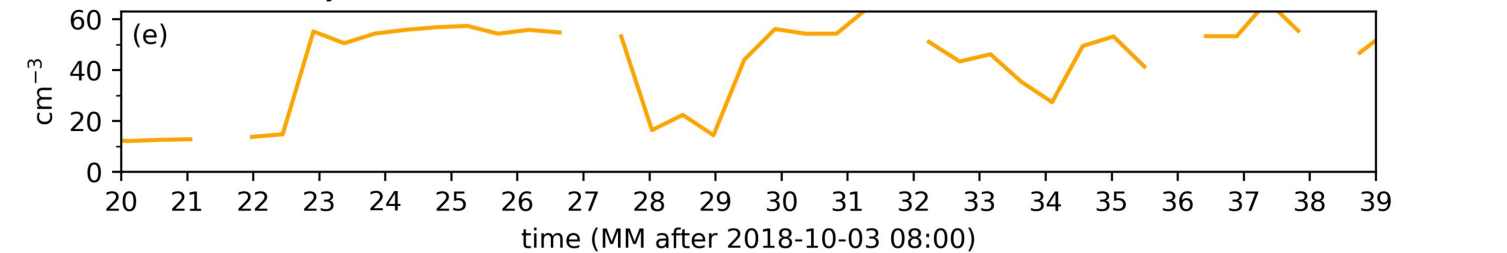


Electric Field Power Spectral Density

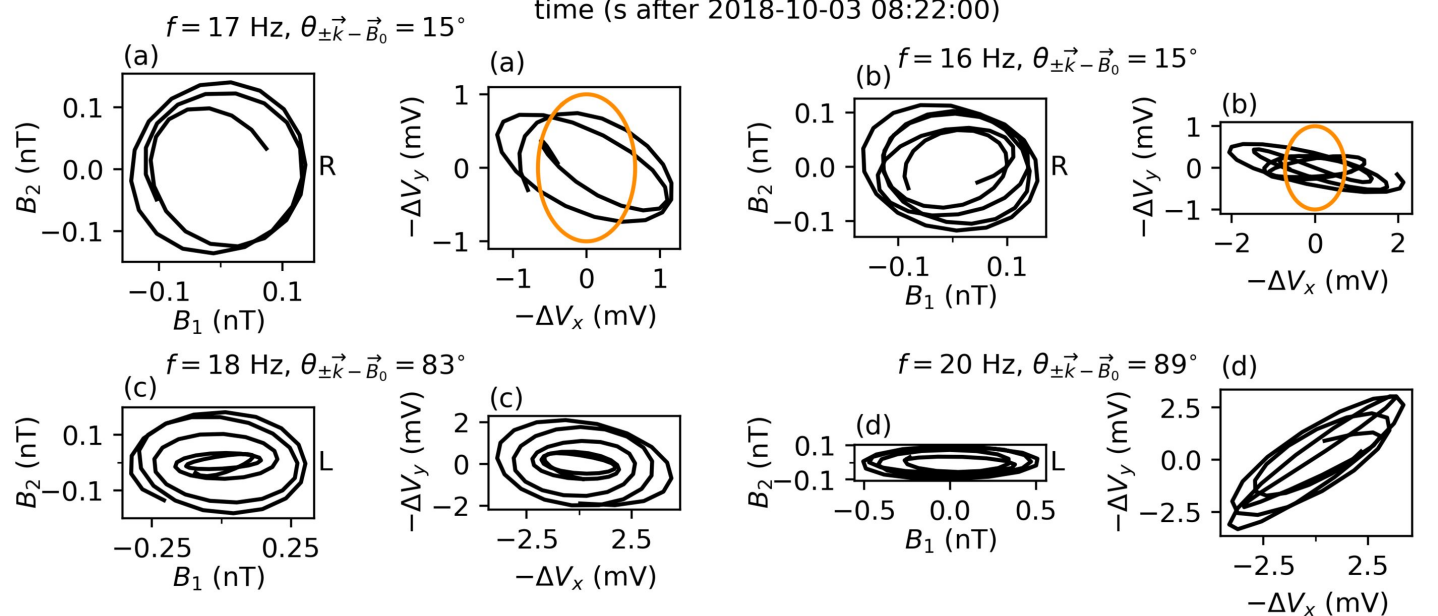
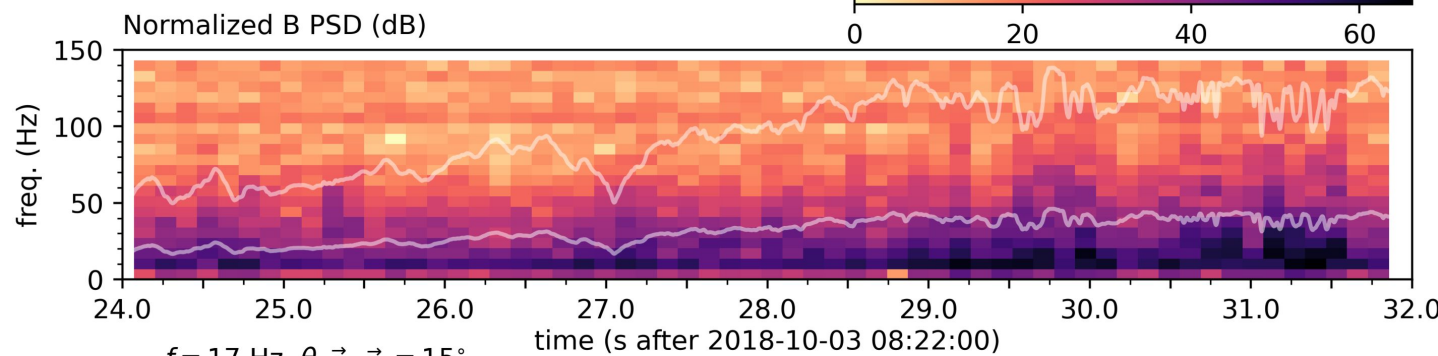
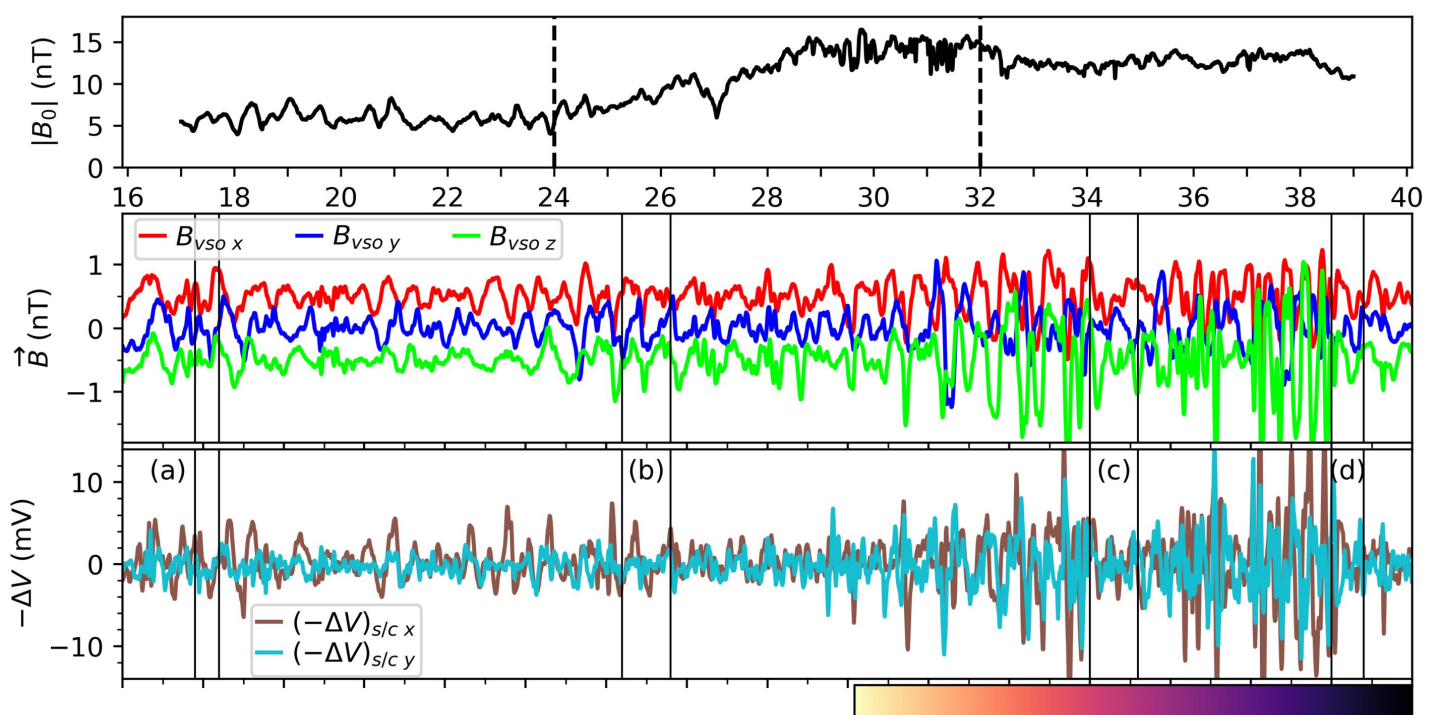
(dB Above Background)



Electron Density



new_bs1_rev2.png.



new_ob_ww_diag.png.

